Railway track location estimation using onboard inertial sensors

Peinado Gonzalo, Alfredo; Entezami, Mani; Roberts, Clive; Weston, Paul; Stewart, Edward; Hayward, Mick; Hsu, Sin Sin

DOI:
10.1080/00423114.2021.1968443

Railway Track Location Estimation using Onboard Inertial Sensors

Alfredo Peinado Gonzalo[a]*, Mani Entezami[a], Clive Roberts[a], Paul Weston[a], Edward Stewart[a], Mick Hayward[b], Sin Sin Hsu[b]

[a]*Birmingham Centre for Railway Research and Education, University of Birmingham, Birmingham, United Kingdom;* [b]*Network Rail High Speed, Kent, United Kingdom*

*Corresponding author: Alfredo Peinado Gonzalo, axp864@student.bham.ac.uk, ORCID Id.: https://orcid.org/0000-0002-2327-2514

Railway Track Location Estimation using Onboard Inertial Sensors

Abstract: In railways, using a track- and ride-quality monitoring system on in-service train has become desirable for coordination and security. Identification of the track- or train-related rough rides via train crew can be estimated to the nearest kilometre. However, if the train is equipped with a monitoring system a better location and track quality evaluation can be provided. These systems commonly use information such as GNSS and/or an odometer to provide location information. This work proposes a practical method for track alignment estimation using real data from an in-cab inertial measurement system and using also a novel method based on crosslevel variations. The speed estimation is done through speed-related harmonics detected on inertial sensors, which depend on speed and track characteristics; and distance correction is provided by comparing crosslevel derived from inertial sensors and a reference track geometry. The effectiveness and accuracy of the method is demonstrated with data collected between London and Ashford.

Keywords: Railway; speed estimation; inertial sensors; track monitoring; crosslevel

1. Introduction

Positioning systems are generally divided into trackside and on-board equipment, aiming to obtain different results [1, 2]. Trackside equipment is usually aimed at train integrity, wheelset monitoring and evaluating vehicles as they pass by the inspection points [3-5]. On-board equipment, such as Global Navigation Satellite Systems (GNSS) and tachometers, is used to identify the location and speed of the vehicle. On-board equipment can be mounted at various locations, such as on the bogie or on the cab floor. Most common sensors are inertial sensors, eddy current sensors, odometers and tachometers [1]. Sensor fusion is commonly used to improve the measurements provided by different sensors, as explained in the paragraphs below.

Tachometers and odometers are commonly installed on trains for speed and distance estimation, respectively, by measuring wheel rotations. Tachometers obtain speed by measuring the rotation rate of the wheel and then multiplying this by the wheel circumference, whilst odometers use the circumference and rotation count to measure distance [6]. Both devices are subject to rail slippage and wear, as slippage affects the relative distance travelled by the wheel with respect to the rail and wear decreases the wheel radius, making it necessary to add correction factors to their estimations or combine them with other devices [7, 8].

Inertial sensors, when used for distance and speed estimation, are usually merged with odometers or GNSS, using Kalman filters [9] to combine and process the data and improve their respective estimations [10]. Kalman filters are used for predicting variables using the mean and covariance of Gaussian distributions, applying matrix calculus to the previous state variables. Mei and Li [11] developed a method to acquire vehicle speed using only a couple of accelerometers located over each wheelset on a bogie. They estimated vehicle speed using the signal delay and knowing the separation between sensors using cross-correlation with a determined time window. This method is susceptible to have signal delay in zones where the vehicle is accelerating or decelerating at low speed, and lack of precision at high speeds due to an inadequate time window. Jiao *et al*. [12] combined inertial sensors and a GPS on a maglev train to improve GPS speed estimation. Their results compare position and speed error to the GPS reference and showed a qualitative improvement on both distance and speed estimation errors when using the Kalman filter. Further applications of sensor fusion are Mazl and Preucil [13], who obtained distance errors below 2 m for 5-minute runs combining GPS and inertial sensors; Cai and Wang [14], who explained their use of a Kalman filter on sensor fusion and compared tests with and without GPS in a square course of side 200 m; Ernest *et al.*

[15], who combined an odometer and inertial sensors to estimate speed and distance when a GPS signal is unavailable; and Malvezzi *et al*. [7, 16, 17], by developing an odometer combining gyroscopes and accelerometers, and simulated runs in different conditions with errors below 3% in estimated position.

Sensor fusion is applied not only between inertial sensors and GNSS, but also with a variety of sensors following different approaches. Liu *et al*. [18] combined signal from GPS and Beidou satellites using a Kalman filter to reduce position estimation error below 25 m along the track. Yufeng *et al.* [19] combined a GPS with both inertial sensors and a Doppler radar on a maglev train; and proposed and simulated a method capable of working stably in the absence of a GPS signal. Saab [20, 21] developed a method to compare estimated vehicle position to a topological track map, by combining yaw rate from a gyroscope and speed from two tachometers via a Kalman filter, and then matching them to a test track, obtaining positioning errors below 2% of the total. Vehicle positioning in absence of GPS data is solved by Jiang *et al.* [22] by combining inertial sensors and an odometer, and comparing them to the track map; and Li *et al.* [23] by combining inertial sensors using an Extended Kalman filter and applying machine learning techniques to several runs on the same track, reducing positioning error significantly compared to original estimations.

A 6-degree of freedom (3-axis acceleration and 3-axis rotation rate) Inertial Measurement Unit (IMU) is used in this work, based on previous projects carried out by the authors and colleagues at the Birmingham Centre for Railway Research and Education (BCRRE). There are several publications focused on its use for railway condition monitoring. Research carried out by Weston *et al*. focuses on monitoring both lateral and vertical track irregularity, installing IMUs on the axlebox and the bogie of Tyne and Wear Metro and Class 175 vehicles [24, 25]. Their results show the possible alternate use of

gyroscopes to measure track irregularities instead of accelerometers and agree with their proposed models. In publications by the same group, the IMU is installed on the bogie in order to observe the evolution and degradation of a track over nine months; explaining the combination of accelerometer and gyroscope signals to measure displacement and the alignment processes for the data [26, 27]. Further applications of the IMU are in Entezami *et al*, referring to the computing of the vertical displacement, data alignment on a transition to a bridge as well as position estimation in tunnels and for ride-quality estimation [28, 29].

This paper focuses on the use of the IMU located in the vehicle cab to obtain the distance along a route and the position of elements within that route, such as faults or switches and crosses, via a novel method based on the harmonics that appear on inertial sensors and the use of crosslevel as a reference. The work was carried out to estimate the speed of the vehicle particularly when neither GNSS or a tachometer are available, using time and frequency domain analyses. Comparing the speed profile of a journey and the spectrogram of the inertial sensors, similarities are observed in the shape of the curve, in particular at frequencies below 25 Hz and above 80 Hz. Movements within vehicle body are related to wheel-track interaction, forces and speed. There is a linear correlation between the speed and the harmonics generated by the movement, as demonstrated in the thesis by Vilhelmsson, in which an Extended Kalman Filter is applied to the vibration signal from a cart to estimate its speed [30]**.**

The conditions of the test (tracks, vehicle and sensors) are presented in Section2. In Section 3, the steps to estimate speed from the frequency response of the sensors and the results for the different sections of the track are explained. Section 4 elaborates the method to adapt distance estimated from the previous section using crosslevel as a

reference and presents the results for the sections of the track. Finally, in Section 5 the conclusions from the investigation are explained and further research is discussed.

2. Track and Test Conditions

The route in which tests have been carried out is between London St Pancras International and Ashford International stations; it is divided into three sections as displayed in Table I. The route and its sections are shown in Figure 1, where the segments without GNSS availability are marked with a white line. Measurements were carried out on a British Class 395 Javelin [31]. Detailed information about the IMU and its performance is available elsewhere [29]. Each test is done with the vehicle starting and ending its travel in a station, so the vehicle speed starts and ends at zero.

Table I. Track sections characteristics.

Section	**Route**	**Distance [km]**	**Average speed [kmh^{-1}]**	**GNSS availability [%]**
1	Ashford – Ebbsfleet	54.2	161	92
2	Ebbsfleet – Stratford	27.1	138	40
3	Stratford – St. Pancras	9.2	73	20

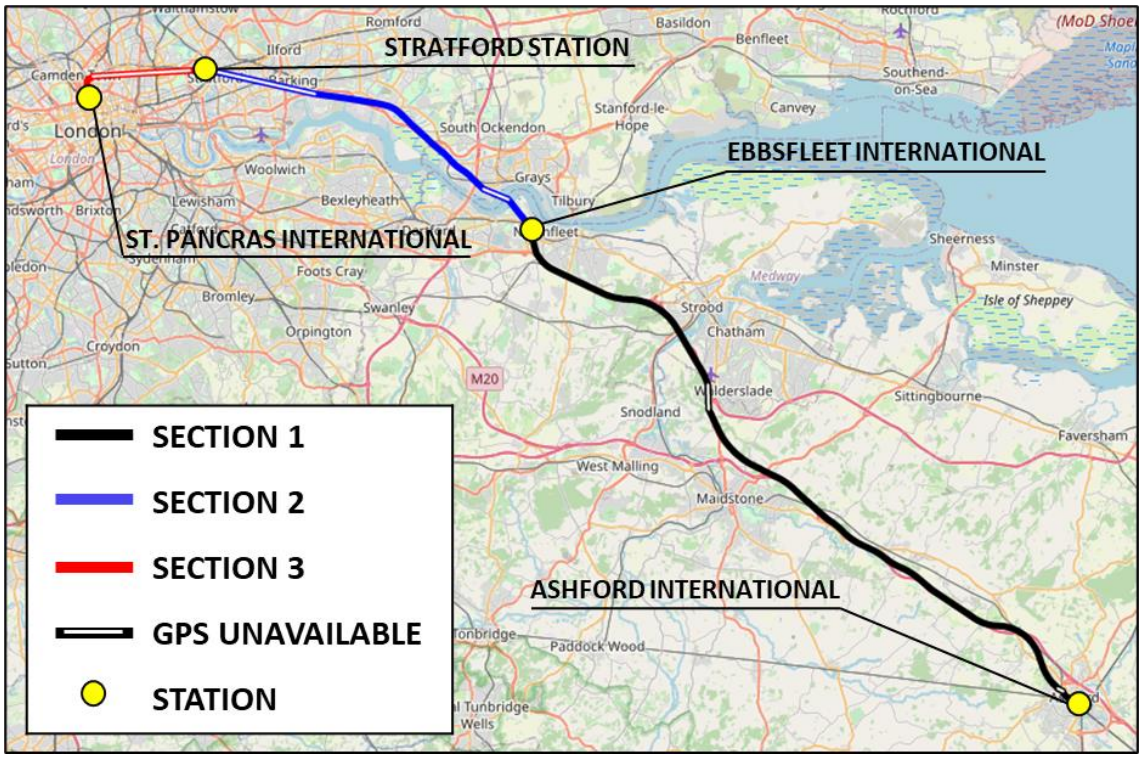

Figure 1. Track route and main sections (from OpenStreetMap).

The device used for the measurements, developed by BCRRE [28] and displayed in Figure 2 left, consists of an IMU with three accelerometers and three gyroscopes measuring in all cartesian directions (Figure 2 right), a GNSS sensor giving speed and geographic location, and a logging system to store the data. The sampling rate of the GNSS is 1 Hz, and 256 Hz for the IMU (down-sampled from 2048 Hz) [32, 33]. Positioning accuracy of the GNSS is generally better than 3 m and speed estimation accuracy 0.1 knots (0.05 ms^{-1}). No other source of information is provided for the measurements, neither tachometers nor odometers.

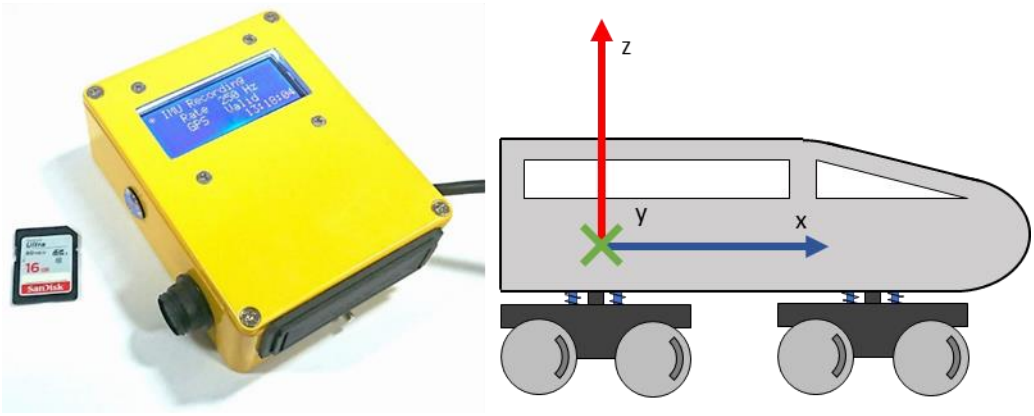

Figure 2. IMU developed by BCRRE [28] (left) and axis system with respect to vehicle (right).

For this piece of research, the longitudinal or X axis corresponds to the direction of travel, the Z axis to the vertical direction and the Y axis to the lateral direction. In the next section, the speed estimation method is discussed.

3. Speed estimation method

This section describes the method to estimate speed using harmonic contents, or resonance frequencies, seen in the sensor channels. These harmonics are caused by vehicle dynamics and wheel vibrations caused by the movement of the train on the track [30]. First, the spectrograms of the sensors are obtained to identify the frequency bands within which observable resonances appear.

Figure 3 shows the full spectrum (0 to 128 Hz) for all the sensors in Section 1 of the track.

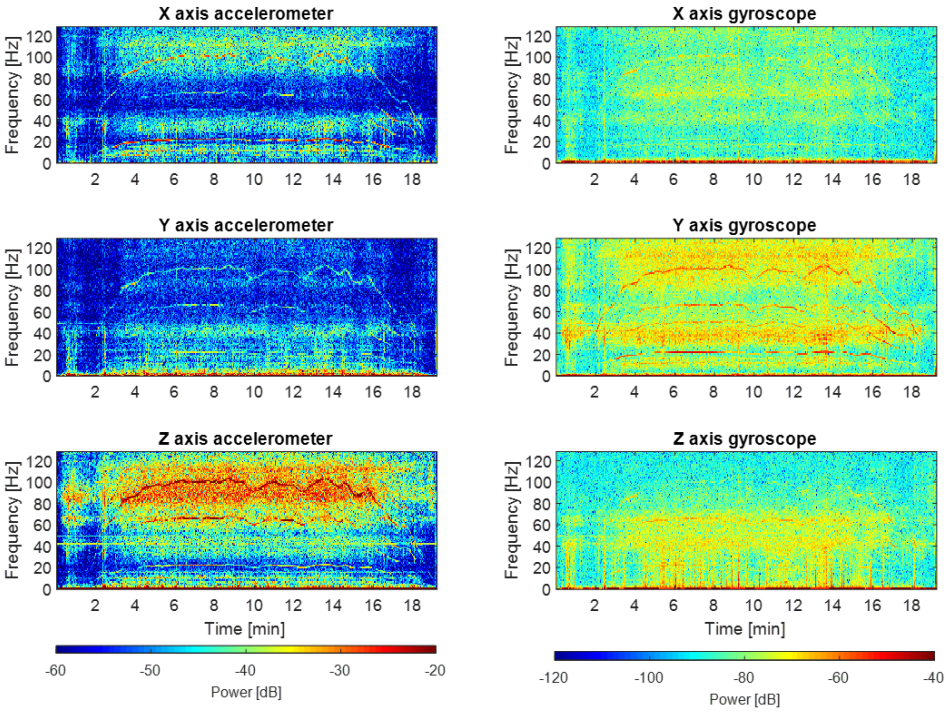

Figure 3. Spectrograms for all inertial sensors.

An analysis of the graphics shows that the best sensors from which it is possible to obtain the resonance points are the X axis accelerometer (a_X), Y axis gyroscope (g_Y) and Z axis accelerometer (a_Z), as their signal to noise ratio is higher than the others; and the best ranges to obtain resonance points are 12 to 25 Hz and 50 to 110 Hz. Hence, these sensor channels and frequency ranges are chosen to obtain the fitting curves from harmonics to speed estimation. These curves are obtained by detecting the power maxima of each time interval and then filtered to avoid high-frequency noise associated

with the fitting.

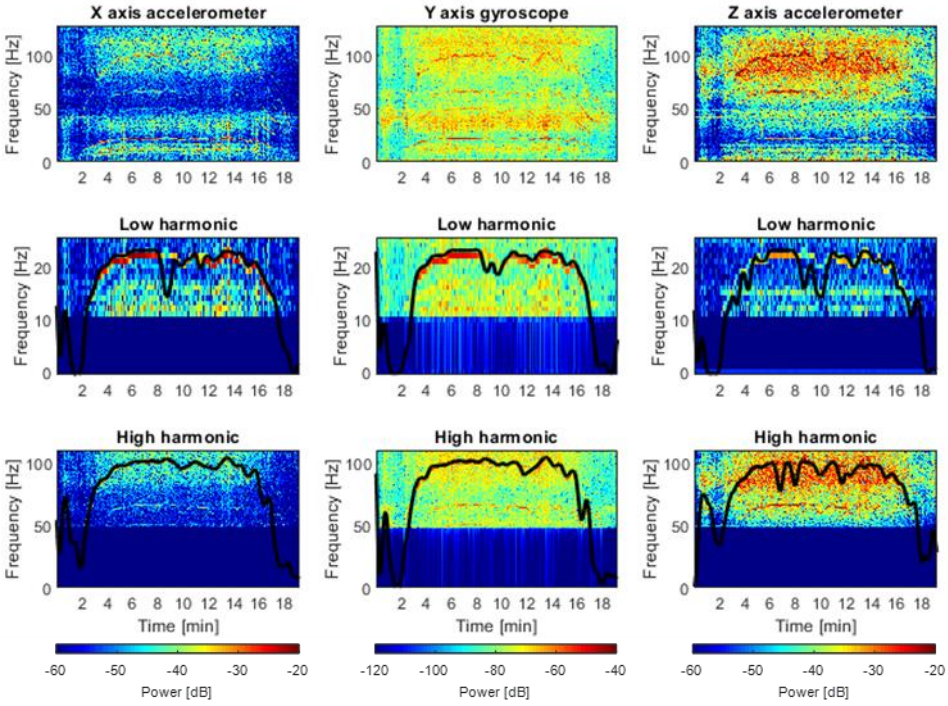

Figure 4 shows the spectrograms of the selected sensors (top) and the fitting curves for the high and low frequency harmonics (center and bottom).

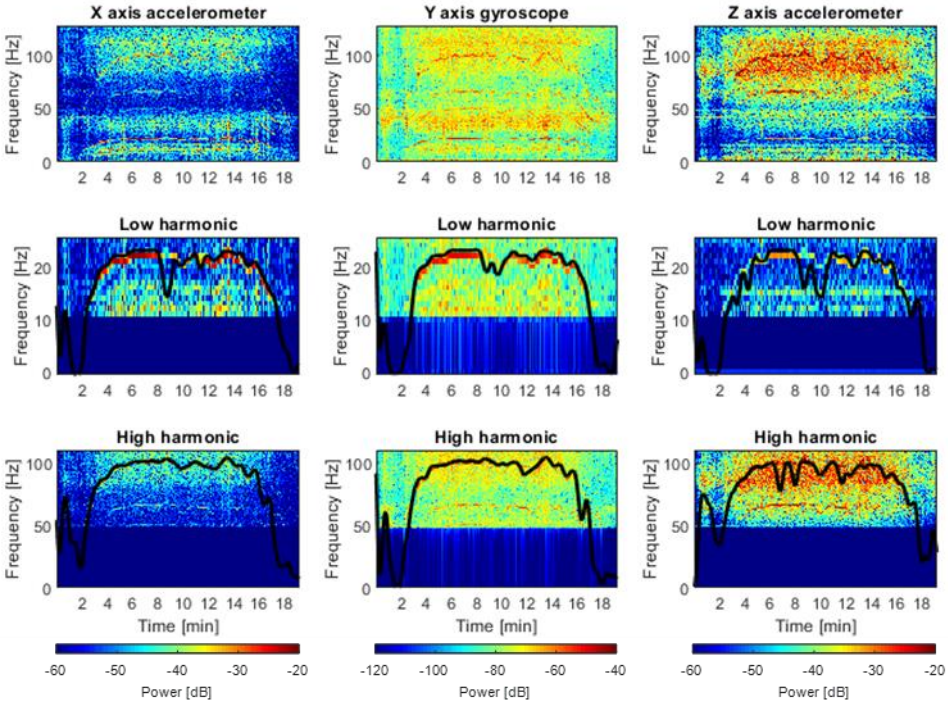

Figure 4. Selected spectrograms and signal curve fitting.

Once the curves have been obtained, a linear scaling factor k is applied to fit them to the vehicle speed magnitude before comparing them to the GNSS reference; defined as $k = s/f$, where s is the vehicle speed in ms^{-1} and f is the harmonic frequency in Hz. This scaling factor is calculated as follows: using track section 1 as it has the best conditions for testing, it is observed that the maximum vehicle speed is approximately 60 ms^{-1} and the maximum value for the low frequencies of about 23 Hz, so the scaling factor is 2.6 m; for the high frequencies the maximum frequency reached is around 100 Hz., so the scaling factor is 0.6 m. The best fitting curve is selected automatically as the one whose cumulative absolute error respect to the GNSS estimation is the lowest of all.

Figure 5 shows the speed estimation for all sensors extracted from the spectra on top, where the selected speed is highlighted with a thicker line width (high harmonic of a_X in this case); and on bottom the comparison between the selected speed and the GNSS estimation, where the segments without available signal are marked with a grey shading. In this case, GNSS signal is unavailable at minute 12 of the test.

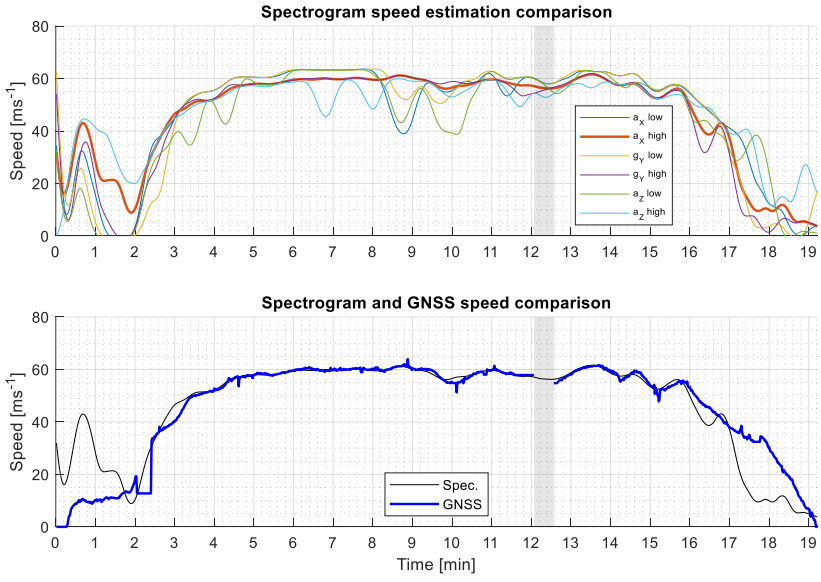

Figure 5. Speed estimation compared to spectrograms (top) and GNSS (bottom).

To improve the estimation, a Kalman filter [9] has been applied combining the speed from the spectrogram and from the GNSS (considering signal availability) and the integral of a_X. The speed from the spectrogram (y_{spec}) and from the GNSS (y_{GNSS}) are considered measurements or signal inputs and the integral of a_X is the correction factor. This integral is corrected using θ_Y, given by Equation (1), to eliminate the influence of gravity when the vehicle is on a slope, given by Equation (2).

$$\theta_{y,t} = \int_0^t \dot{\theta}_y \, dt \quad ; \quad (1)$$

$$\Delta V_t = \left(a_{x,t} + g\,\theta_{y,t}\right)\Delta T \; ; \; (2)$$

where the variation of speed against time (ΔV_t) is the corrected integral of acceleration, applied to correct the previous estimation from the filter; g is the gravitational constant; and $\dot{\theta}_y$ is the pitch rate. The equation is then applied and displayed as follows in Equation (3).

$$\begin{cases} x^*_{t+1} = x_t + \Delta V_t \\ P^*_{t+1} = P_t + Q \end{cases} \; ; \; (3)$$

where x^*_{t+1} and x_t are the a priori and a posteriori predictions, respectively; P^*_{t+1} and P_t are the a priori and a posteriori covariance matrices, respectively; and Q is the process noise covariance matrix. Both predictions and matrices have dimensions 1x1 in this case. This estimation is updated with the innovation factor adding the speed from the spectrogram and the GNSS as a speed vector, considering availability by modifying the covariance measurements matrix R in the system shown in Equation (4).

$$\begin{cases} \eta_{t+1} = \begin{bmatrix} y_{spec} \\ y_{GNSS} \end{bmatrix} - H \cdot x^*_{t+1} \\ S_{t+1} = H \cdot P^*_{t+1} \cdot H' + R \\ K_{t+1} = P^*_{t+1} \cdot H' \cdot S^{-1}_{t+1} \end{cases} \; ; \; (4)$$

where η_{t+1} is the innovation factor; y_{spec} is the estimated speed from the spectrogram; y_{GPS} is the estimated speed from the GNSS; S_{t+1} is the innovation

covariance matrix; H is the measurements matrix and K_{t+1} is the Kalman gain. The correction is finally applied to the predictions as displayed in Equation (5).

$$\begin{cases} x_{t+1} = x^*_{t+1} + K_{t+1} \cdot \eta_{t+1} \\ P_{t+1} = P^*_{t+1} - K_{t+1} \cdot H \cdot P^*_{t+1} \end{cases} ; \quad (5)$$

Figure 6 shows the different estimations and errors using GNSS estimation as reference; it is subjected to its own errors and signal availability, but it is used as reference since it is the only available data. In the segments without GNSS signal, the error estimation is not applicable, as error is calculated based on the GNSS speed values.

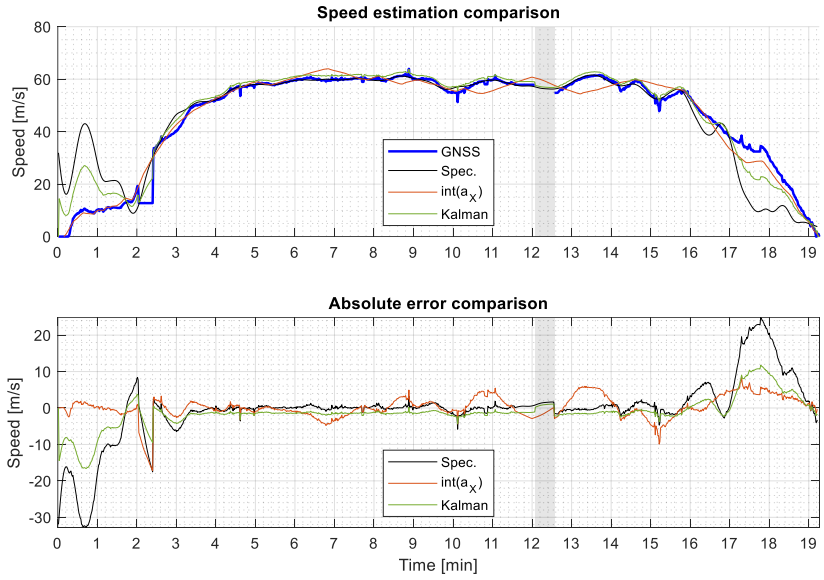

Figure 6. Comparison between speed estimations (top) and errors (bottom).

It is observed that, considering GNSS as reference, the error of the spectrogram estimation is generally below 2 ms^{-1}, and improved with the Kalman filter at high speeds. The speed can also be estimated without GNSS signal, although there is no reference to be compared to. Also, at speeds lower than 20 ms^{-1} the accuracy of the estimations generally decreases. To show the use of the method under different speed and GNSS availability conditions, the following subsections show the results of estimating the speed in the three track sections stated in Section 2.

3.1.Section 1. Ebbsfleet International to Ashford International

This section is above ground and the speed limit is 250 kmh^{-1} (70 ms^{-1}), being the one with most GNSS availability and higher average speed. Figure 7 shows the low frequency range spectrogram of a_X (0-25 Hz) to show the frequency spectrum quality on top, the speed estimation comparison from the GNSS, spectrogram and Kalman filtered estimation on bottom. The GNSS-blank segment of data corresponds to the vehicle running through North Downs Tunnel, close to Walderslade, as shown in Figure 1. Notice the units of the horizontal axis in both subplots are in minutes, in order to enable a comparison in the same domain for both spectrogram and estimations.

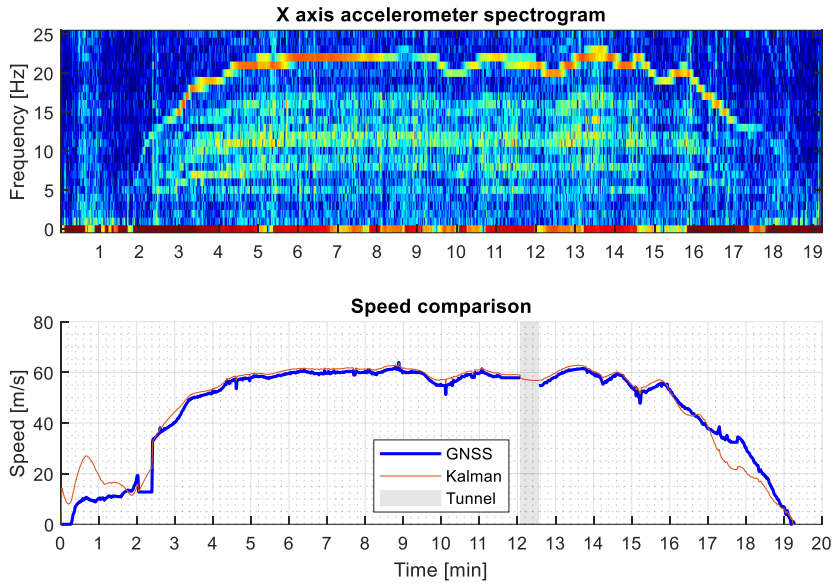

Figure 7. Spectrogram (top) and speed comparison (bottom) for Section 1.

The GNSS signal, where available, allows the comparison between the spectrogram estimation and the GNSS data, which achieved errors usually below 2 ms^{-1} most of the time, having lower accuracy when the speed varies significantly or is below 20 ms^{-1}, suggesting the hypothesis of lower accuracy at lower speeds. This is observed between min 0 to 2 and 17 to 19 and is due to the lower power intensity of the harmonics at low speeds, possibly caused by an unknown resonance phenomena in the vehicle suspension.

3.2.Section 2. Stratford Station to Ebbsfleet International

This section is underground as the vehicle passes through the River Thames. Hence, GNSS availability is approximately 50% of the route. Figure 8 shows the spectrogram of a_X on top, and the speed estimation comparison from the GNSS, spectrogram and Kalman filtered estimation on bottom. The segments without GNSS signal are marked as shaded areas; they are located in minutes 2 to 5 and at minute 9 approx. These segments correspond to the London underground and the vehicle passing under the Thames, as presented in Figure 1. As these segments have no reference speed from the GNSS the error cannot be estimated properly.

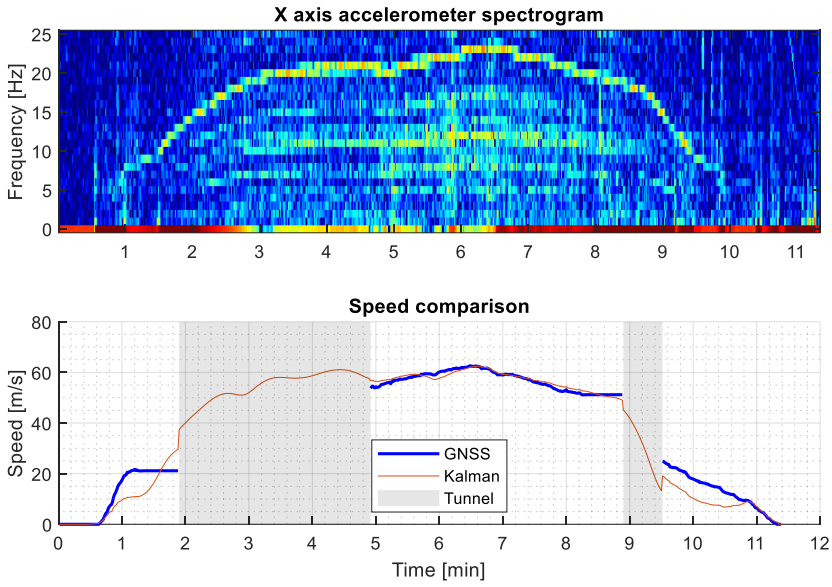

Figure 8. Spectrogram (top) and speed comparison (bottom) for Section 2.

In this case, the speed estimation is worse than in the previous section, as the vehicle runs generally at a lower and varying speed and GNSS availability is lower. Higher frequency harmonics disappear at minutes 1 to 3 and 6 to 9, as observed in the top graphic, while the vehicle passes through tunnels. The error is generally below 5 ms^{-1} at speeds from 40 to 60 ms^{-1}, ranging then from 8 to 12% of train speed. From these observations, it can be stated that the speed estimation is more accurate at speeds higher

than 20 ms^{-1}, as observed in track section 1. It is also observed that the zones in which there is no GNSS signal available, generally tunnels, correspond to zones in which there are no higher harmonics, implying that the type of track is likely to affect the appearance of some harmonics.

3.3.Section 3: St. Pancras International to Stratford Station

This section is mainly underground in London; therefore its GNSS availability is poor (less than 20%), and the vehicle speed is the lowest of all the track sections. The intensity and definition of the signal is low, hindering speed estimation. Figure 9 shows the spectrogram of the X axis accelerometer from 0 to 25 Hz and the comparison between GPS and Kalman estimation, highlighting the tunnel as the grey shaded area.

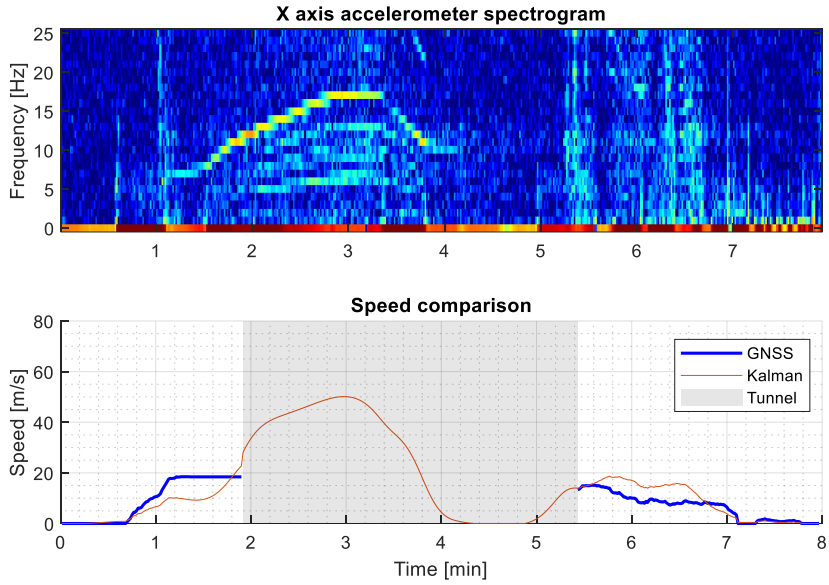

Figure 9. Spectrogram (top) and speed comparison (bottom) for Section 3.

The observable harmonics appear only on the low range of frequencies, at approximately 20 Hz, so the scaling factor of 2.6 m is applied to them. This estimation is mostly done using only the spectrogram, as no GNSS is available most of the track, so the error

comparison can only be done in a small part of the section. This error is observed to be up to 5 ms^{-1} compared respect to GNSS estimation (where available), at a speed of 10 ms^{-1}. Hence, the estimation can be considered inaccurate for low speeds, which has approximately 50% error where signal is available.

3.4.Comments

The appearance of harmonics has been detected using frequency analysis, producing a curve with a shape similar to the speed estimated from the GNSS (Figure 8 shows this effect clearly). These harmonics are more visible on the X and Z axis accelerometers and the Y axis gyroscope, so only these sensors have been used for the speed estimation method. There are four main harmonics which, at a constant speed of 60 ms^{-1} (top speed of the vehicle), are at approximated frequencies of 23, 50, 66 and 100 Hz. These values produce ratios speed to frequency of 2.6, 1.2, 0.9 and 0.6 m. It is believed that the 2.6 and 1.2 ratios are related to the bogie wheelbase, which is 2.6 m.

It is also observed that tunnels remove the appearance of all the harmonics but the lowest one and filter the frequency band between 60 and 100 Hz. The speed of the vehicle also seems to have an influence on the appearance of the harmonics, as they lose intensity and become indistinguishable from the background noise below 20 ms^{-1}. It is also worth mentioning that acceleration is much reduced as lower speeds so the accelerometers tend to have a much reduced signal at lower speeds, so this may be considered an influencing factor.

The causes of the appearance of the harmonics are not clear. However, it is observed that both g_Y and a_Z are related to the vertical movement of the vehicle, harmonics disappear at speeds below 20 ms^{-1} and higher frequency harmonics disappear in tunnels. These observations imply an influence of the movement of the vehicle on harmonic appearance, particularly on the vertical direction.

From this section, it is concluded that an accurate estimation of the train speed is possible considering the frequency response of the inertial sensors. Finally, the integral of this speed estimation is then applied to estimate the distance along track. The following section proposes a method to improve the estimated distance using a reference crosslevel provided by the infrastructure manager (Network Rail).

4. Using Crosslevel to assist with alignment

This section presents the process to improve the estimated distance from the previous section based on the use of crosslevel from a reference and the IMU, and aligning them; considering crosslevel as the time integral of the roll rate or the difference in height between two adjacent rails [34]. To do this, it is first necessary to obtain crosslevel from the IMU data and the reference. Figure 10 shows the estimated speed and the crosslevel from the IMU and the reference against distance.

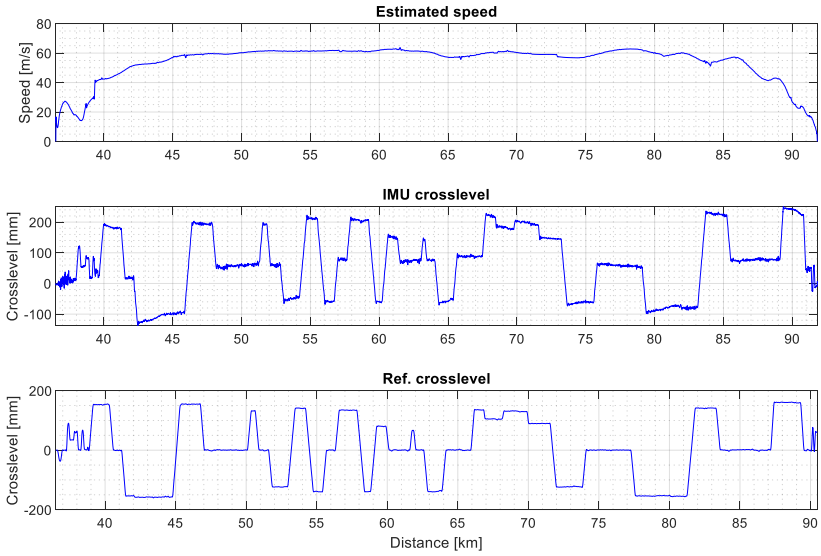

Figure 10. IMU estimated speed (top), IMU estimated crosslevel (center) and reference (bottom).

Once crosslevel data have been obtained, transitions between constant crosslevels are identified automatically using the time derivative of crosslevel, namely the roll rate, for both the IMU and the reference. Figure 11 shows the identified and numbered crosslevel transitions for both IMU and reference at the start of a section, in which transitions are highlighted with a grey shading. Differences between the amount and location of transitions are observed comparing both subfigures, due to the lack of accuracy of the distance estimation obtained from the previous section. Numbering is carried out to identify false positives or transitions not related between IMU and reference, since false positives are preferred to false negatives for this processing. Once unwanted transitions are identified, they are supressed manually.

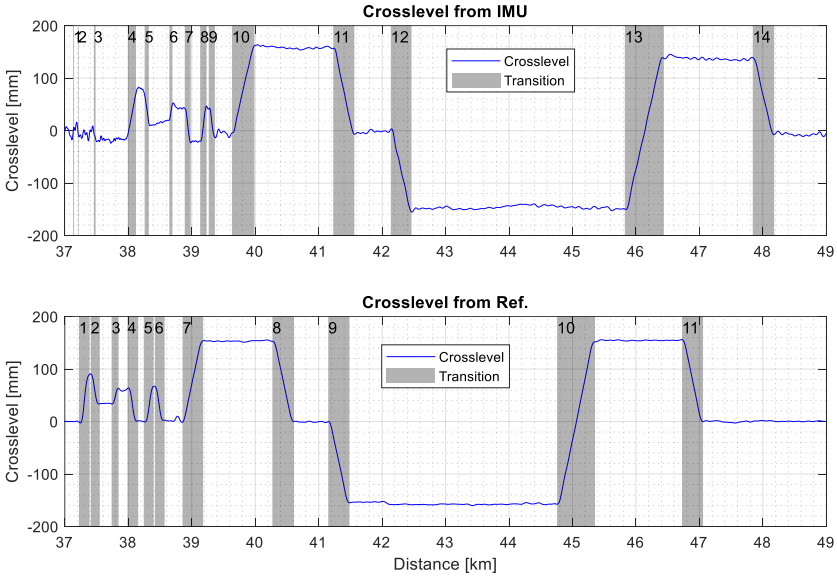

Figure 11. Detail of crosslevel and identified transitions from IMU (top) and reference (bottom).

Once transitions have been correctly selected, a preliminary step must be taken to remove the vertical drift in the data which is caused by sensor noise, amplified with the integration of the signal. This drift cannot be corrected using digital filters, as the wavelength of the drift is too large to be removed; nor considering a unique slope, as it is

not linear, although this slope is used as an auxiliary parameter. To eliminate drift, the dataset is separated into segments of constant crosslevel and crosslevel transitions, as presented in Figure 12. For each segment, a straight line is calculated to remove the vertical drift, where the start point of each segment is equal to the endpoint of the previous one. This line is labelled as 'Trend'. The slope of each segment is computed as follows: if the segment is a crosslevel transition, only the general slope is used to remove the vertical drift; if it is a constant crosslevel segment, the slope is computed from the height difference between start and endpoints of the crosslevel estimation and then removed from the data segment. Figure 12 shows the crosslevel before detrending, together with the Trend in vertical dimension on top, and crosslevel after correction and the zero-crosslevel line (neutral line) on bottom.

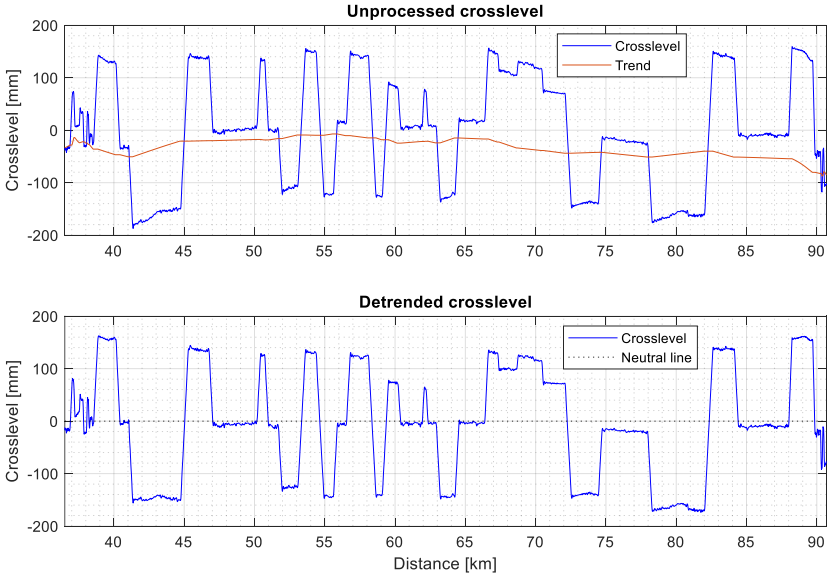

Figure 12. Crosslevel estimation before (top) and after detrending (bottom).

Finally, crosslevel is corrected horizontally, resampling each segment between points from the original length to the length of the reference using linear interpolation. Due to the processing and resampling, small overshoots may appear on the crosslevel signal. This problem is solved by applying a low pass filter on the processed crosslevel.

Figure 13 shows a comparison between the reference and IMU crosslevel before (top) and after processing (centre) and the estimated error per segment of the processing (bottom).

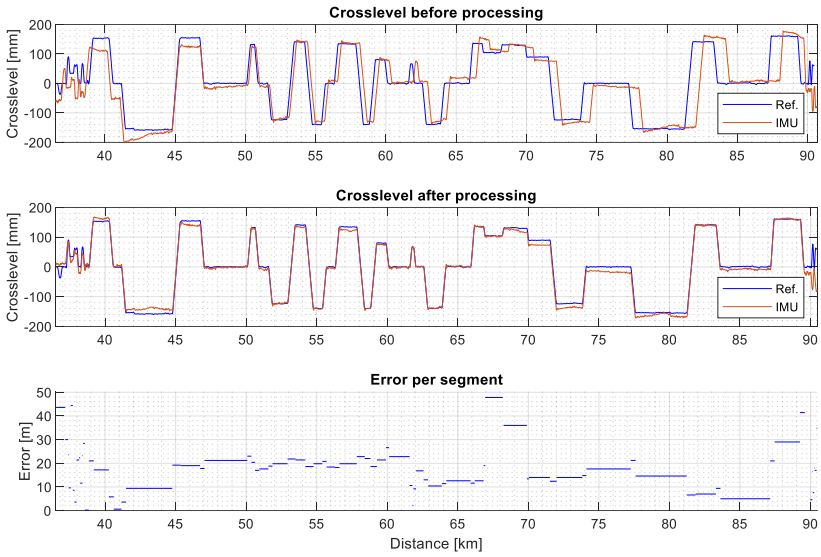

Figure 13. Crosslevel comparison before (top) and after processing (center) and estimation errors (bottom).

In order to show an example of application, Figure 14 shows a comparison of the vertical displacement measured by the train before and after crosslevel alignment, in which sensor data is complemented with the location of switches and crosses as vertical black lines and tunnels as shaded areas. Both subfigures show that several tunnels cause overshoots in the signal, as well as the apparition of segments with high displacement levels that may indicate track degradation; but the improved estimation shows more accurately the location of these overshoots, generally in the same track length as tunnels or tunnel entrances.

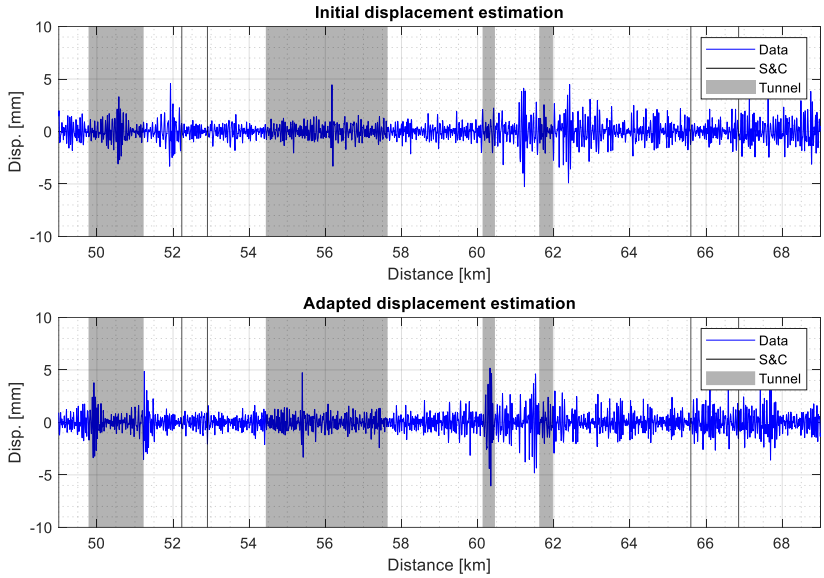

Figure 14. Vertical displacement comparison before (top) and after crosslevel alignment (bottom).

The following subsections show the distance adaptation using crosslevel for the track sections stated in Section 2, in order to show compare the accuracy of the estimations from Sections 3.1 to 3.3 to the correction presented in this section. Of course, comparison against GNSS distance/position cannot be carried out because of the lack of GNSS availability. Ideally, estimated distance should be similar to the reference provided.

4.1.Section 1. Ebbsfleet International to Ashford International

This section has the highest GNSS signal availability and it appears to be the fastest section; therefore, the initial distance estimation is expected to be accurate. The dataset used for this case study is the one employed to show the crosslevel alignment method, so the observations are the same. They are summarized as follows: There is a notable vertical drift in the signal and misalignments between the distance estimation from the IMU and the reference before processing. After the correction is applied, both drift and misalignment have been removed. There is an error per segment in the order of

20 m in most of the track segments, which tends to be lower in the longer ones; the magnitude of this error shows that the crosslevel alignment method is accurate enough to be used.

4.2.Section 2: Stratford Station to Ebbsfleet International

This section has GNSS availability on 50% of the track length and the average speed is lower than on the previous section, so the initial estimation is expected to be worse. Figure 15 shows the crosslevel comparison between reference and IMU before and after processing and the relative error per segment.

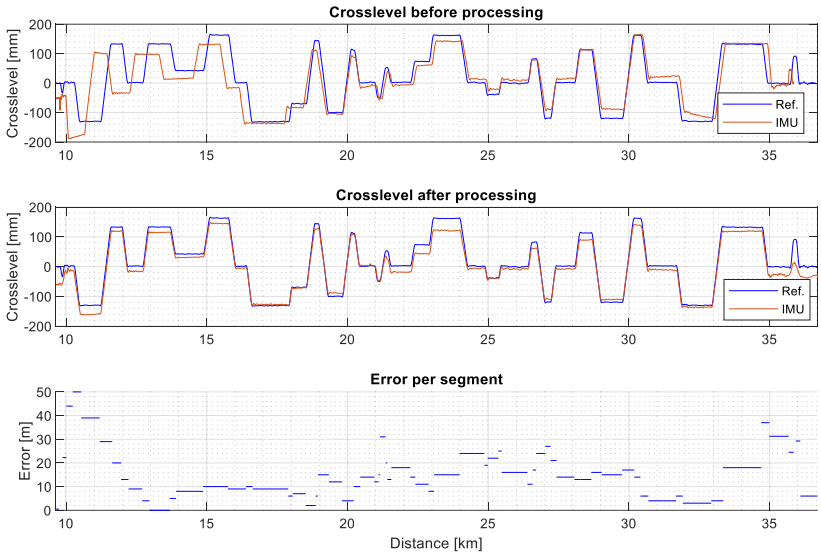

Figure 15. Crosslevel comparison before (top) and after processing (center) and errors (bottom) for Section 2.

Similar to the previous section, there is a varying drift in the initial estimation and the error magnitude is roughly 20 m. it is also observed that error tends to be lower in large segments of track than in short ones. Hence, there seems to be consistency in the error per segment obtained.

4.3.Section 3: St. Pancras International to Stratford Station

This section is in the underground London. The initial distance estimation is expected to be inaccurate as vehicle speed is generally low. Figure 16 shows the crosslevel comparison between reference and IMU before and after processing and the relative error per segment.

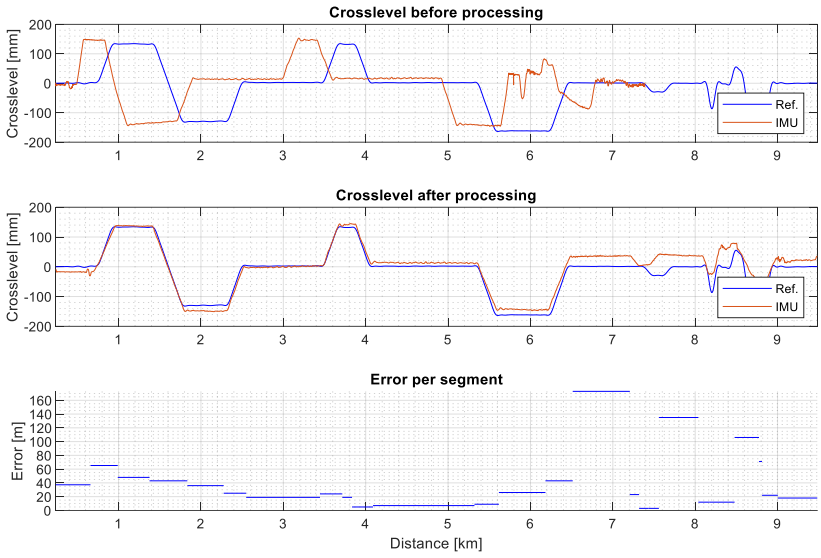

Figure 16. Crosslevel comparison before (top) and after processing (center) and errors (bottom) for Section 3.

The results show that the initial distance estimation is not accurate, as the estimation error is highly above 40 m. The adaptation also shows errors beyond 170 m, implying low effectiveness in some segments. There are false negatives in the identified transitions before correcting the distance estimation; this could be considered as a reason to change the threshold to detect them for each dataset, although doing so could reduce the possibilities to automate the processing. Therefore, a balance between the threshold and the possibilities to have false negatives has to be considered.

From the results and figures presented above, it can be concluded that the method to improve distance estimation using crosslevel as a reference is accurate enough to be

useful for further research and for position estimation of any identified element of the track that requires inspection.

5. Conclusions

This work has defined a novel method to estimate speed using harmonics detected on inertial sensors on high-speed railway vehicles, and adapt the distance estimated from the speed using crosslevel as a reference. The estimation method combined these harmonics with GNSS estimated speed and vehicle acceleration using a Kalman filter to achieve errors below 5 ms^{-1} (8% approx.) at vehicle speeds above 40 ms^{-1}, although this estimation is worse when speed is low or varying.

The causes of the apparition of these harmonics have not been identified yet. However, the frequency analysis shows a correlation of them with vehicle speed and a possible connection with vertical track irregularities and wheel-track interaction, as discussed in Section 3. This connection is supported by the high intensity of the signal on the Z axis accelerometer and the Y axis gyroscope, and the disappearance of the harmonics at speeds below 20 ms^{-1}, that generate less vibration on the cab. As previously stated, there are other causes that may affect the appearance of these harmonics, such as the signal-to-noise ratio of the inertial sensors.

A novel method to adapt distance estimation using crosslevel has also been presented. This method uses abrupt changes in crosslevel to detect transitions between constant crosslevel segments and adapt the distance using a reference provided by the infrastructure manager. This method provides estimation errors usually below 20 m on track segments spanning kilometres, so its accuracy has also been demonstrated. Thus, the method can be applied for dataset comparison on tracks to observe their evolution and degradation reliably.

Further work to be done for this research is the development of optimal criteria to select the harmonics used for the speed estimation and the use of the rest of harmonics for a more accurate estimation; and to automate how to correlate crosslevel transitions detected in the IMU and the reference. This automation could be then applied to align and compare data from different runs to observe track evolution. It would be also useful to discover the causes of the harmonic apparition in order to investigate if these harmonics appear in other train models and other conditions. Finally, further challenges to be addressed are the need to increase the method accuracy at low speeds and to study its accuracy where no GNSS signal is available as there is no speed reference.

Acknowledgements

The work is funded by the Engineering and Physical Sciences Research Council (EPSRC) through the research Track to the Future (EP/M025276). The authors would like to thank Network Rail High Speed for their support throughout this project.

References

1. Otegui, J., et al., *A survey of train positioning solutions.* IEEE Sensors Journal, 2017. **17**(20): p. 6788-6797.
2. Hamid, H.A., G.L. Nicholson, and C. Roberts, *Impact of train positioning inaccuracies on railway traffic management systems: framework development and impacts on TMS functions.* IET Intelligent Transport Systems, 2020. **14**(6): p. 534-544.
3. Kouroussis, G., et al., *Review of trackside monitoring solutions: from strain gages to optical fibre sensors.* Sensors, 2015. **15**(8): p. 20115-20139.
4. Alemi, A., F. Corman, and G. Lodewijks, *Condition monitoring approaches for the detection of railway wheel defects.* Proceedings of the Institution of Mechanical Engineers, Part F: Journal of Rail and Rapid Transit, 2017. **231**(8): p. 961-981.
5. Ni, Y.-Q. and Q.-H. Zhang. *A Bayesian Machine Learning Approach for Online Wheel Condition Detection Using Track-side Monitoring*. in *2018 International Conference on Intelligent Rail Transportation (ICIRT)*. 2018. IEEE.
6. British Standards Institution, *BS 3403:1972: Indicating tachometer and speedometer systems for industrial, railway and marine use*. 1972, United Kingdom.

7. Malvezzi, M., et al. *Train position and speed estimation by integration of odometers and IMUs*. in *9th World Congress on Railway Research, Lille, France*. 2011.
8. Jiang, Q., et al., *A new filtering and smoothing algorithm for railway track surveying based on landmark and IMU/odometer.* Sensors, 2017. **17**(6): p. 1438.
9. Kalman, R.E., *A new approach to linear filtering and prediction problems.* Journal of basic Engineering, 1960. **82**(1): p. 35-45.
10. Mirabadi, A., N. Mort, and F. Schmid. *Application of sensor fusion to railway systems*. in *1996 IEEE/SICE/RSJ International Conference on Multisensor Fusion and Integration for Intelligent Systems (Cat. No. 96TH8242)*. 1996. IEEE.
11. Mei, T. and H. Li, *Measurement of vehicle ground speed using bogie-based inertial sensors.* Proceedings of the Institution of Mechanical Engineers, Part F: Journal of Rail and Rapid Transit, 2008. **222**(2): p. 107-116.
12. Jiao, Y., et al. *Research on Maglev Train Positioning System Based on Multi-Information Fusion*. in *2018 2nd IEEE Advanced Information Management, Communicates, Electronic and Automation Control Conference (IMCEC)*. 2018. IEEE.
13. Mazl, R. and L. Preucil. *Sensor data fusion for inertial navigation of trains in GPS-dark areas*. in *IEEE IV2003 Intelligent Vehicles Symposium. Proceedings (Cat. No. 03TH8683)*. 2003. IEEE.
14. Cai, B. and X. Wang, *Train positioning via integration and fusion of GPS and inertial sensors.* WIT Transactions on the Built Environment, 2000. **50**.
15. Ernest, P., R. Mazl, and L. Preucil. *Train locator using inertial sensors and odometer*. in *IEEE Intelligent Vehicles Symposium, 2004*. 2004.
16. Malvezzi, M., B. Allotta, and M. Rinchi, *Odometric estimation for automatic train protection and control systems.* Vehicle system dynamics, 2011. **49**(5): p. 723-739.
17. Malvezzi, M., et al., *A localization algorithm for railway vehicles based on sensor fusion between tachometers and inertial measurement units.* Proceedings of the Institution of Mechanical Engineers, Part F: Journal of Rail Rapid Transit, 2014. **228**(4): p. 431-448.
18. Liu, J., et al. *A GPS/compass based train integrated positioning method for high-speed railways*. in *2012 IEEE-APS Topical Conference on Antennas and Propagation in Wireless Communications (APWC)*. 2012. IEEE.
19. Yufeng, L., C. Tefang, and C. Shu. *Processing and Fusion of Velocity and Position Signal of Medium and High Speed Maglev Train*. in *2018 13th World Congress on Intelligent Control and Automation (WCICA)*. 2018. IEEE.
20. Saab, S.S., *A map matching approach for train positioning. I. Development and analysis.* IEEE Transactions on Vehicular Technology, 2000. **49**(2): p. 467-475.
21. Saab, S.S., *A map matching approach for train positioning. II. Application and experimentation.* IEEE Transactions on Vehicular Technology, 2000. **49**(2): p. 476-484.
22. Jiang, W., et al., *A Multi-Sensor Positioning Method-Based Train Localization System for Low Density Line.* IEEE Transactions on Vehicular Technology, 2018. **67**(11): p. 10425-10437.
23. Li, D., X. Jia, and J. Zhao, *A Novel Hybrid Fusion Algorithm for Low-Cost GPS/INS Integrated Navigation System During GPS Outages.* IEEE Access, 2020. **8**: p. 53984-53996.

24. Weston, P., et al., *Monitoring vertical track irregularity from in-service railway vehicles.* Proceedings of the institution of mechanical engineers, Part F: Journal of Rail and Rapid Transit, 2007. **221**(1): p. 75-88.
25. Weston, P., et al., *Monitoring lateral track irregularity from in-service railway vehicles.* Proceedings of the Institution of Mechanical Engineers, Part F: Journal of Rail and Rapid Transit, 2007. **221**(1): p. 89-100.
26. Yeo, G., P. Weston, and C. Roberts, *The utility of continual monitoring of track geometry from an in-service vehicle.* 2014.
27. Weston, P., et al., *Perspectives on railway track geometry condition monitoring from in-service railway vehicles.* Vehicle System Dynamics, 2015. **53**(7): p. 1063-1091.
28. Entezami, M., et al., *Lineside and on-board monitoring techniques for infrastructure and rolling stock on high-speed lines.* The International Journal of Railway Technology, 2017. **6**.
29. Entezami, M., et al. *Continuous railway track monitoring using passenger trains*. in *World Congress on Railway Research*. 2019. Tokyo, Japan.
30. Vilhelmsson, R., *Vibration analysis for speed estimation of wheeled indoor vehicles*. 2017.
31. Hitachi Ltd. *Class 395 (Javelin)*. 2021 [cited 2021 March]; Available from: http://www.hitachirail-eu.com/products/projects/class-395-javelin.
32. *Garmin GPS 18x OEM | Sensor*. 2021 [cited 2021 March]; Available from: https://www.garmin.com/en-GB/.
33. Analog Devices. *ADIS16460 (Rev. C)*. 2020 [cited 2021 March]; Available from: https://www.analog.com/en/products/adis16460.html.
34. British Standards Institution, *BS EN 13848-1:2019: Railway Applications: Track. Track geometry quality*. 2019, United Kingdom.